Fabrication of GMR Magnetic Field Sensing Devices for Air-gap Flux Measurements in SRMs

Thong Chi Le[1], Hargsoon Yoon[2], Roy McCann[3] and Vijay Varadan[3]

[1] Ho Chi Minh City University of Technology, Ho Chi Minh City, Vietnam
[2] Norfolk State University, Norfolk, VA 23504, USA
[3] University of Arkansas, Fayetteville, AR 72701, USA

Abstract

This paper describes the development of magnetic field sensing devices using giant magnetoresistance (GMR) effect. The sensor contains multilayered magnetic nanowires containing alternating ferromagnetic and nonmagnetic layers. Multilayered nanostructures with Co and Cu layers were fabricated using pulsed electrochemical deposition to control the periodic structure of nanolayers in a nanopore template. The use of the sensor is to provide for air-gap flux measurements in switch reluctance motors (SRMs).

1. Introduction

Recent studies on switched reluctance machines (SRMs) have attracted ongoing attention by researchers in the area of electrical energy conversion. The SRM offers many advantages compared to conventional machines for variable-speed industrial drives due to advantages such as an inherently rugged construction, wide operating speed range, fault tolerant operation, and reduced material and manufacturing costs. The deployment of SRMs by industry for variable-speed drive applications, however, has been slow due to issues with torque ripple and acoustic (audible) noise. It is also noted that SRM designs that maximize torque production while minimizing overall mass and volume constraints for aerospace and ground vehicle applications usually mandates very small air-gap dimensions between the rotor and stator. This results in stringent manufacturing requirements for lamination tolerances. In addition, SRMs require complex control algorithms to incorporate feedback of shaft position and phase current (I. Husain, 2002).

Today, most advanced control techniques for electrical machinery is based on an equivalent circuit model derived at the machine electrical terminals. As an alternative, researchers are considering the use of embedded magnetic field sensors to observe and control the operation of electric machines from direct measurements of instantaneous machine air-gap flux levels. Providing for air-gap flux measurements in SRMs is challenging due to the small air-gap dimensions as well as the large flux density gradients ranging between high saturation to nearly zero magnetization (W. F. D. Traore, T. C. Le, R. McCann, 2007). This paper presents the results of developing an air-gap magnetic field sensor device that meets these demanding requirements in order to provide for improved operation of SRMs.

2. SRM control techniques

SRMs are gaining wider popularity among variable speed drives due to their inherent simplicity, ruggedness, and extensive development (I. Husain, 2002). However, SRMs require complex control techniques to operate. Depending on the number of the motor phase as well as the desired control algorithm, numerous power stage topologies are used, in particular, a power stage with two independent power switches per motor phase. It is necessary to know the position of the rotor to commutate the motor phase. The position feedback can be produced by using position sensors, such as encoders, Hall sensors, etc. Several sensorless control methods are reported by many researchers, most of which involve evaluation of the variation of magnetic circuit parameters that are dependent on the rotor position (Switched Reluctance Motor).

Two main characteristics of a high performance SRM drive is torque ripple minimization and energy optimization (C. Mademlis, I. Kioskeridis, 2003). In order to reduce the torque ripple, there are primarily two approaches.

The first method is to improve the magnetic design of the motor by changing the stator and rotor pole structures. But this can be done only at the expense of some specific motor outputs. Kavanagh *et al.* (R. C. Kavanagh, J. M. D. Murphu, M. Egan, 1991) introduced mechanical modifications in the polar regions of SRM, so that the machine can operate with a smooth torque. Radun (A. V. Radun, 1995) presented analytical equations designed for SRM, which can be used to design the machine with optimized geometry to reduce the torque oscillation.

The second method is to use sophisticated electronic control techniques, which is based on optimizing the control parameters including the supply voltage, turn-on and turn-off angles, and current levels. By using electronic control techniques, the minimization of torque ripple may reduce the average torque since the motor capabilities are not being fully utilized at all power levels (I. Husain, 2002). According to several research papers, there are numerous control methods for SRM performance optimization. They can be categorized in two main control architectures including the average and instantaneous torque control. The average torque control is developed on per-stroke basis and the time-averaged analysis of machine operation is used in this control. The instantaneous torque control is based on continuous difference of phase current references within stroke duration and control angles (C. Mademlis, I. Kioskeridis, 2003). The instantaneous torque is computed by taking the derivative of the co-energy, as shown in Equation (1). Because of the magnetic nonlinearities of an SRM, the output electromagnetic torque of the machine can be described by nonlinear torque-current-angle (τ-i-θ) data, which are experimentally measured from the motor. Therefore the highly nonlinear nature of SRM makes it difficult to apply formal optimization techniques for optimizing the torque ripple (N. Bhiwapurkar, T. K. A. Brekken, N. Mohan, 2006), (R. A. McCann, M. S. Islam, I. Husain, 2001).

$$\tau = \frac{\partial W}{\partial \theta} = \tau(i_a, i_b, i_c, \theta) \quad (1)$$

where τ is the torque developed in motor.

i_a, i_b, i_c are the phase currents.

θ is the rotor position.

McCann *et al.* presented a new approach for real-time torque estimation and rotor position estimation that provides a solution to the most pressing issues related to SRM applications (R. McCann and W. Traore, 2008), (W. F. D. Traore, 2008). They investigated the ability to estimate instantaneous torque from a sampling of direct measurements of the air-gap flux density. The method computes the Maxwell stress tensor in real-time based on magnetic flux measurements from embedded flux sensors. The magnetic field sensors are based on the giant magnetoresistive (GMR) effect and provide the instantaneous magnetic field level in the air-gap of the machine during operation. By observing the flux density measured from the GMR sensors and torque profiles obtained from finite element analysis (FEA) results at each rotor position, McCann *et al.* hypothesized that the SRM torque can be written as the product of three terms:

$$\tau = k \cdot B_{av} \cdot B_{sav} \quad (2)$$

where k is a coefficient to adjust for the torque exact value.

B_{av} is the average value of the flux density magnitude.

B_{sav} is the average value of all the slopes of flux density for a given current value.

In their work (R. McCann and W. Traore, 2008), the coefficient k will generally be a function of the rotor position and the average slope is computed by taking the difference in flux measured by each adjacent pair of GMR sensors.

Therefore this research associated with the work of McCann *et al.* will improve the performance of switched reluctance machines and make it suitable for automotive and industrial applications.

3. Development of multilayered magnetic nanowires for GMR sensors

3.1 Materials

Polycarbonate ion-track etched nanopore membranes with pores of 100 and 200 nm diameter and pore density of 4×10^8/cm^2 were purchased from Whatman Co. S1805 photoresist and MF319 developer from Microchem Corp. were used for LATB process. A $Na_3Au(SO_3)_2$ (TechniGold 25ES) solution from Technic Inc was used as received for electrochemical deposition of gold. For electrochemical deposition of cobalt and copper, $CoSO_4$, $CuSO_4$ and H_3BO_3 were purchased from Sigma Aldrich. An IM6eX electrochemical system (Zahner Elektrik) was used to control galvanometric and potentiometric pulse of electrochemical processes. A platinum wire mesh worked as a counter electrode and an Ag/AgCl electrode was used as the reference electrode.

3.2 Multilayered Nanowire Growth

Electrodeposition refers to the deposition of a pure metal or alloy from an electrolyte solution by the passing of an electric current. The morphology of deposited nanowires depends on several factors including electrolyte composition, pH, temperature, and deposition potential. Here, a pulsed technique

was used to grow eletrodeposited multilayered nanowires, which are ideally suited for studying GMRs. Co/Cu structures was applied, because the electrochemical reduction potential of two materials are sufficiently far apart to permit separate electrodeposition of both materials in a single electrolyte.

Before electrochemical deposition, a 5 nm layer of Cr and 330 nm layer of Au were deposited on a silicon or polyimide substrate by electron-beam evaporation and electroplating. A polycarbonate nanopore membrane with 47 mm diameter was then placed and attached on the substrate by applying S-1805 photoresist. The cylindrical nanopores on the polycarbonate membrane were then selectively opened by modified lithography process. Detailed test results regarding the adjusted lithography process are explained in (H. Yoon, D. D. Desphande, V. Ramachandran, V. K. Varadan, 2008).

Co/Cu multilayered structures were prepared from a single electrolyte bath. The electrolyte, is confined to the up side of the membranes, contains 250g/l $CoSO_4 \cdot 7H_2O$, 0.25g/l $CuSO_4 \cdot 5H_2O$, and 30g/l H_3BO_3. This solution has pH value of 3.89 and the pH was controlled by H_2SO_4, or NaOH. Co and Cu were deposited at -1.0V and -0.5V, respectively, relative to the Ag+/AgCl reference electrode. At -0.5V, only Cu is deposited, whereas at -1.0V, both Cu and Co are co-deposited. However, because of the very low Cu concentration (Cu concentration < 2%), nearly pure magnetic layers can be obtained. Many studies have been reported on the preparation and characterization of electrodeposited Co/Cu multilayers in which the magnetic layer is, as a result of the nature of the electrodeposition method, not pure Co but rather a Co-rich Co-Cu alloy with magnetic properties very similar to those of pure Co. Due to the deposition rate of Co is much faster than that of Cu, only a small amount of Cu is co-deposited in the Co layer.

During the deposition, the applied potentials are set by the electrochemical workstation IM6ex, which integrates the amount of charge passing between the working electrode and the counter electrode. The potential is switched when the amount of charge corresponding to a designed layer thickness is reached. By applying a sequence of voltage pulses between −0.5V and -1.0V, it is possible to grow multilayered structures, where the thickness of the magnetic and non-magnetic layers is controlled by the duration of the respective voltage pulses.

After growing nanowires, the sample was then flushed continuously with DI water and the polycarbonate membrane was dissolved by using the Remover PG solution and was cleaned with IPA and DI water. These nanowire arrays obtained after dissolution of the membranes were observed by a scanning electron microscope (SEM). X-ray diffraction (XRD) was used to determine the characteristic of the crystal structure of Co nanowires in the arrays.

3.3 Electrical connection on nanowires

Electrical connection to a single Co/Cu nanowire involves further Co deposition on the tip of nanowires and monitoring of resistance between nanowires and the top electrode using a DC multimeter. After the polycarbonate membrane bonding process, the top electrode was patterned on the top side of membrane using e-beam evaporation and hard mask. Since top electrode lines with Ti (200 nm) and Au (50 nm) layers completely block the

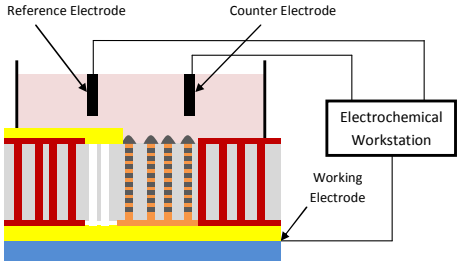

(a)

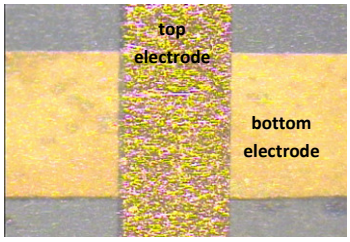

(b)

Fig. 1. (a) Schematic diagram of electrode connection and (b) top view image of the bottom and top electrodes.

pores, Co/Cu multilayered nanowires can be grown only outside the electrode area as shown in figure 4. After fabrication of multilayered nanowires inside membrane using a pulsed mode, rest of pore space was filled by Co nanowires growth until outgrowth tip is formed on the membrane surface. At the final

step, the small gap between the outgrowth tip and top electrode was filled by subsequent Co deposition at -1.0 V and the resistance change was monitored by a DC multimeter. By measuring the resistance between the two electrodes, we were able to monitor their connection and separation. When the growing of Co decreased the gap between the top electrode and a nanowire, the resistance between the two electrodes dropped drastically. Upon further deposition and making contact, the resistance changes in discrete steps and finally reaches to stable value at the minimum.

3.4 Experimental results and discussion

For multilayered Co/Cu nanowire growth, pulsed potential repeatedly switched between -0.5V and -1.0V was applied. Deposition currents for Cu at -0.5V and for Co at -1.0V were measured around 200 μA/6 cm^2 and 16 mA/6 cm^2, respectively. Open circuit control was applied between each pulse for 10 seconds. This periodic interval can provide displacement reaction of Cu nobler than Co (S. Valizadeh, L. Hultman, J.M. George, P. Leisner, 2002), (T. M. Whitney, P. C. Searson, J. S. Jiang, C. L. Chien, 1993), (Q. Liu, J. H. Min, J. U. Cho, Y. K. Kim, 2005). Displacement reaction can dissolves weak bonding Co sites from the surface and allow Cu coating on the surface without faradic reaction. This reaction may favor building higher crystalline structure along the nanowires.

In Fig. 2, arrays of multilayered nanowires with Co Fig. 2 presents an SEM image of arrays of nanowires with Co layer and Cu layer. In order to improve crystalline structure, open circuit control steps allowing displacement reaction were applied. It was observed that the crystalline structures along the (002) plane were significantly improved as shown in Fig. 3.

After the fabrication process, a precision bipolar magnet controller from Walker Scientific Inc. was used to apply a variable external magnetic field in order to measure the GMR effect. The resistance of nanowires was recorded when the magnetic field is changed from 0 to ±10,000 Oe. The resistance of 417 Ω at zero magnetic fields decreased when increasing the magnetic field. The GMR result of 2.4% was observed when applying the external magnetic field parallel to the axis of nanowires (Fig. 4). The working range of this device is about from -5,000 Oe to 5,000 Oe. Similar results were obtained on multiple devices. Even though careful control of the electrochemical growth process by monitoring the resistance change is required, this technique for

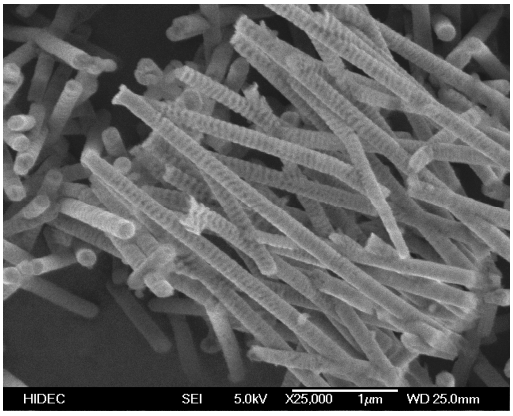

Fig. 2. SEM image of multilayered Co/Cu nanowires.

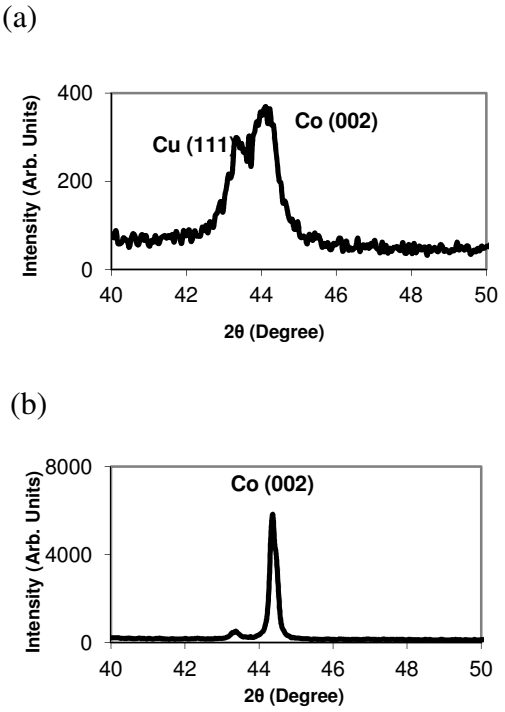

Fig. 3 X-ray diffraction patterns of multilayered Co/Cu without open circuit control (a) and with open circuit control (b).

building device structures is highly favorable for nanowire device development for industrial applications due to the high range of applied magnetic field.

4. Conclusions

The main contribution of this research is the design and fabrication of magnetic field sensors based on

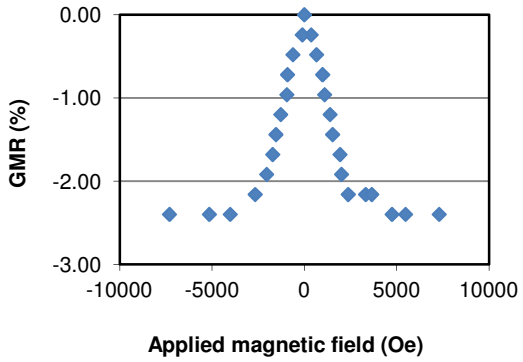

Fig. 4. The GMR results of 100-nm diameter Co/Cu multilayered nanowires when applying external magnetic field.

GMR effect for magnetic field measurements in industrial applications. These applications often require sensors capable of measuring fields of up to several kOe. Although GMR effect was developed by Albert Fert and Peter Grünberg in 1988 (M. N. Baibich, J. M. Broto, A. Fert, F. Nguyen Van Dau, F. Petroff, 1988), (G. Binsasch, P. Grünberg, F. Saurenbach, W. Zinn, 1989), and GMR sensors were first created by IBM in 1994 (Jim Belleson, Ed Grochowski, 1998), GMR sensors are widely used in computer hard drive as reading heads which are used in low range of field. The detection range of these sensors is around a few militesla (mT). Our GMR magnetic sensing devices are capable of detecting high range of magnetic field which is suitable the design and fabrication of sensors to be embedded into a prototype motor as a means to significantly improve the efficiency, power density and controllability of reluctance-based electrical machines.

References

A. V. Radun. (1995). Design Consideration for the Swicthed Reluctance Motor. *IEEE Transaction on Industry Applications , 31* (5), 1079-1087.

C. Mademlis, I. Kioskeridis. (2003). Performance Optimization in Switched Reluctance Motor Drives with Online Commutation Angle Control. *IEEE Transactions on Energy Conversion , 18* (3), 448-457.

G. Binsasch, P. Grünberg, F. Saurenbach, W. Zinn. (1989). Enhanced magnetoresistance in layered magnetic structures with antiferromagnetic interlayer exchange. *Physical Review B , 39* (7), 4828 - 4830.

H. Yoon, D. D. Desphande, V. Ramachandran, V. K. Varadan. (2008). Aligned nanowire growth usinglithography-assisted bonding of a polycarbonate template for neural probe electrodes. *Nanotechnology , 19*, 025304 (8pp).

I. Husain. (2002). Minimization of Torque Ripple in SRM Drives. *IEEE Transactions on Industrial Electronics , 49* (1), 28-39.

Jim Belleson, Ed Grochowski. (1998). Retrieved from The era of giant magnetoresistive heads: http://www.hitachigst.com/hdd/technolo/gmr/gmr.htm

M. N. Baibich, J. M. Broto, A. Fert, F. Nguyen Van Dau, F. Petroff. (1988). Giant Magnetoresistance of (001)Fe/(001)Cr Magnetic Superlattices. *Physical Review Letters , 61* (21), 2472-2475.

N. Bhiwapurkar, T. K. A. Brekken, N. Mohan. (2006). Torque Ripple Optimization of Switched Reluctance Motor Using Two-phase Model and Optimization Search Techniques. *Power Electronics Specialists Conference, 2006. PESC apos;06. 37th IEEE*, (pp. 1-6).

Q. Liu, J. H. Min, J. U. Cho, Y. K. Kim. (2005). The pH dependence of Co-Cu alloy thin films fabricated on amorphous substrate by DC electrodeposition. *IEEE Trans. Mag. , 41*, 930-932.

R. A. McCann, M. S. Islam, I. Husain. (2001). Application os Sliding Mode Observer for Switched Reluctance Motor Drives. *IEEE Trans. on Industry Applications , 37* (1), 51-58.

R. C. Kavanagh, J. M. D. Murphu, M. Egan. (1991). Torque Ripple Minimization in Switched Reluctance Drives using Self-Learning Techniques. *Proc. of IECON'91*, *1*, pp. 289-294.

R. McCann and W. Traore. (2008). Investigation of Direct Flux Measurements in Switched Reluctance Motors. *Power and Energy Society General Meeting - Conversion and Delivery of Electrical Energy in the 21st Century, 2008 IEEE*, (pp. 1-7).

S. Valizadeh, L. Hultman, J.M. George, P. Leisner. (2002). Template Synthesis of Au/Co Multilayered Nanowires by Electrochemical Deposition. *Advanced Functional Materials , 12*, 766-772.

Switched Reluctance Motor. (n.d.). Retrieved Jan. 13, 2009, from Freescale Semiconductor: http://www.freescale.com/webapp/sps/site/overview.jsp?nodeId=02nQXGrrlPb02R

T. M. Whitney, P. C. Searson, J. S. Jiang, C. L. Chien. (1993). Fabrication and magnetic properties of arrays of metallic nanowires. *Science , 261*, 1316-1319.

W. F. D. Traore. (2008). *Switched Reluctance Motor Torque and Position Estimation.* Fayetteville: University of Arkansas.

W. F. D. Traore, T. C. Le, R. McCann. (2007). *Real-Time Control of Electric Machines using Embedded Magnetic Field Sensors.*